

Thermally-Assisted Spin-Transfer Torque Dynamics in Energy Space

D. Pinna,^{1,*} A. D. Kent,¹ and D. L. Stein^{1,2}

¹*Department of Physics, New York University, New York, NY 10003, USA*

²*Courant Institute of Mathematical Sciences,
New York University, New York, NY 10012, USA*

Abstract

We consider the general Landau-Lifshitz-Gilbert theory underlying the magnetization dynamics of a macrospin magnet subject to spin-torque effects and thermal fluctuations. Thermally activated dynamical properties are analyzed by averaging the full magnetization equations over constant-energy orbits. After averaging, all the relevant dynamical scenarios are a function of the ratio between hard and easy axis anisotropies. We derive analytically the range of currents for which limit cycles exist and discuss the regimes in which the constant energy orbit averaging technique is applicable.

I. INTRODUCTION

More than a decade has passed since the switching effects of spin-polarized currents traversing nanomagnets were first explored experimentally¹⁻⁴. The quest to characterize how a current may be used to transfer spin-angular momentum into a magnetic system has led to sweeping advances in the field of spintronics. The study and development of spin-valves and magnetic tunnel junctions (see, for example,⁵) with the aim of constructing denser and more efficient memory technologies is one important result of spin-transfer-torque related research. Theoretical treatments usually begin by treating the magnetization within the ferromagnetic film as a single macrospin⁶. Spin-torque effects are then taken into account phenomenologically by modifying the macrospin's dynamical Landau-Lifshitz-Gilbert (LLG) equation¹.

At the nanoscale size, however, one must extend the deterministic treatment described above to include random forces due to thermal noise. The effects of noise become even more pronounced at low currents. A comprehensive theoretical treatment therefore requires taking into account the interplay between noise and the deterministic dynamics. The analysis of such effects is complicated by the non-conservative nature of the spin-torque interaction.

The energetics underlying the thermally activated behavior of uniaxial macrospins have been studied in simple situations both analytically and numerically⁷⁻¹⁰, the latter is possible because of significant computational improvements in graphics processing unit (GPU) technology. The advantage of using a uniaxial macrospin model is that its thermally activated switching dynamics can be modeled using a 1D stochastic differential equation (SDE), which is solvable via standard statistical methods. In practical applications, though, magnets possess a hard axis away from which magnetization deviations have an energy cost. This is particularly true in thin film nanomagnets where, due to the shape of the sample, out of plane magnetizations are energetically suppressed.

Upon adding a hard axis anisotropy to the macrospin model, one is forced to deal with three coupled SDEs. A complete solution is then obtainable only numerically. Nonetheless, a useful approximation can be employed whenever the conservative precessional timescale is small compared to the diffusion timescale, the latter determined by the interplay between noise and spin transfer dynamics. This approximation allows for the construction of a constant-energy orbit averaged (CEOA) LLG equation, which characterizes the macrospin

dynamics by focusing on its slow diffusion in energy space.

An early attempt that used the above approach consisted in writing down a Fokker-Planck equation describing the energy diffusion of the biaxial monodomain^{12,13}. Unfortunately, an energy diffusion equation of this type remains almost as intractable as the original set of dynamical equations. Nonetheless, Apalkov and Visscher¹² estimated a linear exponential scaling ($\log \tau \propto (1 - I)$) between current and mean switching time for thermal switching. However, research work done on uniaxial monodomains has found that, in contrast to the scaling form above, the dependence of mean switching time on current — written generally as $\log \tau \propto (1 - I)^\beta$ — depends on whether one is studying a uniaxial or a biaxial macrospin model. For the former, the exponent β was found to be 2 rather than 1^{8,10,15}.

Alternatively, an effective Langevin equation for the energy dynamics of a uniaxial macrospin can also be constructed by averaging the magnetization dynamics over constant energy trajectories¹⁵. Newhall and Vanden-Eijnden¹¹ numerically constructed an analogous Langevin equation for the energy dynamics of a biaxial macrospin and found numerical evidence for the appearance of stable limit cycles in the macrospin dynamics for certain current regimes. Their analysis supported the Apalkov-Visscher linear scaling result ($\beta = 1$)¹², and demonstrated a current dependence of β for thermal switching starting from a stable limit cycle state. These differing results implied that the transition between the uniaxial and biaxial macrospin models had to be either continuous or at most display a finite discontinuity. Taniguchi¹⁴, by also approximating the Fokker-Planck equation over constant energy trajectories, showed how the exponent β differs from the result of Apalkov and Visscher in the thermally activated regime, as well as from the results of Newhall and Vanden-Eijnden for applied currents greater than a certain critical value. Above this value, β ceases to be constant and instead varies nonlinearly as a function of applied current.

In this paper we extend the energy Langevin approach¹⁵ in order to study the biaxial macrospin model. We obtain analytical expressions for three critical current values across which transitions between different dynamical regimes occur. Two of these are found to be identical to those independently derived by Taniguchi via different means¹⁴. The third critical current sets a limit on the current regimes for which CEOA is a valid approximation. Our analysis explains the transition between the biaxial and uniaxial macrospin regimes, thus shedding light on the contradictory conclusions obtained in the previous literature. We further apply our analytical approach to thermally activated switching and obtain an

analytical expression for the non-linear exponential scaling discussed by Taniguchi¹⁴.

II. GENERAL FORMALISM

A simple model of a ferromagnet uses a Stoner-Wohlfarth monodomain with magnetization \mathbf{M} whose properties are fixed by its shape anisotropy. The energy landscape experienced by \mathbf{M} is generally described by three terms: an applied field \mathbf{H} , an easy-axis anisotropy energy U_K with axis along $\hat{\mathbf{n}}_K$ (Fig. 1) in the $\mathbf{e}_x - \mathbf{e}_z$ plane making an angle θ with the \mathbf{e}_z axis, and a hard-axis anisotropy energy U_p with normal direction $\hat{\mathbf{n}}_D$ perpendicular to $\hat{\mathbf{n}}_K$. The magnetization \mathbf{M} is assumed to be constant in magnitude and for simplicity normalized into a unit direction vector $\mathbf{m} = \mathbf{M}/|\mathbf{M}|$. A spin-polarized current J enters the magnetic body in the $-\mathbf{e}_y$ direction, with spin polarization η , and spin direction along the \mathbf{e}_z axis. The current exits in the same direction, but with its average spin direction aligned along \mathbf{M} . The self-induced magnetic field of the current is ignored here because the dimension a is considered to be smaller than 100 nm, where spin-current effects are expected to become dominant over those due to the current-induced magnetic field. The dynamics are described by the standard LLG equation:

$$\begin{aligned} \dot{\mathbf{m}} = & -\gamma' \mathbf{m} \times \mathbf{H}_{\text{eff}} - \alpha \gamma' \mathbf{m} \times (\mathbf{m} \times \mathbf{H}_{\text{eff}}) \\ & - \gamma' j \mathbf{m} \times (\mathbf{m} \times \hat{\mathbf{n}}_p) + \gamma' \alpha j \mathbf{m} \times \hat{\mathbf{n}}_p, \end{aligned} \quad (1)$$

where $\gamma' = \gamma/(1+\alpha^2)$ is the Gilbert ratio, γ is the usual gyromagnetic ratio and $j = (\hbar/2e)\eta J$ is the spin-angular momentum deposited per unit time with $\eta = (J_\uparrow - J_\downarrow)/(J_\uparrow + J_\downarrow)$ the spin-polarization of incident current J . The last two terms describe a vector torque generated by current polarized in the direction $\hat{\mathbf{n}}_p$. These are obtained by assuming that the macrospin absorbs angular momentum from the spin-polarized current only in the direction perpendicular to \mathbf{m} .¹

To write \mathbf{H}_{eff} explicitly, we must construct an energy landscape for the magnetic body. There are three main components that need to be considered: a uniaxial anisotropy energy U_K , a hard-axis anisotropy U_P and a pure external field interaction U_H . These are written as follows:

$$U_K = -K(\hat{\mathbf{n}}_K \cdot \mathbf{m})^2 \quad (2)$$

$$U_P = K_P(\hat{\mathbf{n}}_D \cdot \mathbf{m})^2 \quad (3)$$

$$U_H = -M_S V \mathbf{m} \cdot \mathbf{H}_{ext} \quad (4)$$

In these equations, M_S is the saturation magnetization, K_P is the hard-axis anisotropy, $K = (1/2)M_S V H_K$, H_K is the Stoner-Wohlfarth switching field (in units of Teslas) and \mathbf{H}_{ext} is the externally applied magnetic field. The full energy landscape then becomes $U(\mathbf{m}) = U_K + U_P + U_H$ and reads:

$$U(\mathbf{m}) = K [D(\hat{\mathbf{n}}_D \cdot \mathbf{m})^2 - (\hat{\mathbf{n}}_K \cdot \mathbf{m})^2 - 2\mathbf{h} \cdot \mathbf{m}], \quad (5)$$

where $D \equiv (K_P/K)$, $\mathbf{h} = \mathbf{H}_{ext}/H_K$ and $\hat{\mathbf{n}}_K$ is the unit vector pointing in the orientation of the uniaxial anisotropy axis. Such an energy landscape has stable magnetic configurations parallel and anti-parallel to $\hat{\mathbf{n}}_K$. The effective interaction field \mathbf{H}_{eff} is then given by

$$\mathbf{H}_{eff} = -\frac{1}{M_S V} \nabla_{\mathbf{m}} U(\mathbf{m}) = -H_K [D(\hat{\mathbf{n}}_D \cdot \mathbf{m})\hat{\mathbf{n}}_D - (\hat{\mathbf{n}}_K \cdot \mathbf{m})\hat{\mathbf{n}}_K - \mathbf{h}], \quad (6)$$

and the deterministic LLG dynamics can then be expressed as:

$$\begin{aligned} \dot{\mathbf{m}} &= -\mathbf{m} \times [(\hat{\mathbf{n}}_K \cdot \mathbf{m})\hat{\mathbf{n}}_K - D(\hat{\mathbf{n}}_D \cdot \mathbf{m})\hat{\mathbf{n}}_D + \mathbf{h}] \\ &\quad - \alpha \mathbf{m} \times [\mathbf{m} \times ((\hat{\mathbf{n}}_K \cdot \mathbf{m})\hat{\mathbf{n}}_K - D(\hat{\mathbf{n}}_D \cdot \mathbf{m})\hat{\mathbf{n}}_D + \mathbf{h})] \\ &\quad - \alpha I \mathbf{m} \times (\mathbf{m} \times \hat{\mathbf{k}}) + \alpha^2 I \mathbf{m} \times \hat{\mathbf{k}}, \end{aligned} \quad (7)$$

where we have defined $I = j/(\alpha H_K)$, introduced the natural timescale $\tau = \gamma' H_K t$, and have chosen our z-axis to be aligned with the spin polarization axis ($\hat{\mathbf{k}} \equiv \hat{\mathbf{n}}_p$).

In practice, the uniaxial and hard-axis axes cannot simply be oriented in any given direction but are, in fact, perpendicular (see Fig. 1). We can write the equations of motion for the magnetization in a rotated coordinate system, where $\hat{\mathbf{n}}_K$, $\hat{\mathbf{n}}_D$ and $\hat{\mathbf{n}}_O$ define our new coordinate system. Let $\hat{\mathbf{n}}_K = (n_x, 0, n_z)$, $\hat{\mathbf{n}}_D = (n_z \sqrt{1-n^2}, n, -n_x \sqrt{1-n^2})$ and $\hat{\mathbf{n}}_O = (-n_z n, \sqrt{1-n^2}, n_x n)$ be the orientation of the uniaxial and hard-axis anisotropy vectors with respect to our original coordinate system (where $n_z = \cos \theta$, $n_x = \sin \theta$ and $n = \sin \phi$). We can then write the dynamical equations in terms of the projections $q \equiv \hat{\mathbf{n}}_K \cdot \mathbf{m}$, $s \equiv \hat{\mathbf{n}}_D \cdot \mathbf{m}$ and

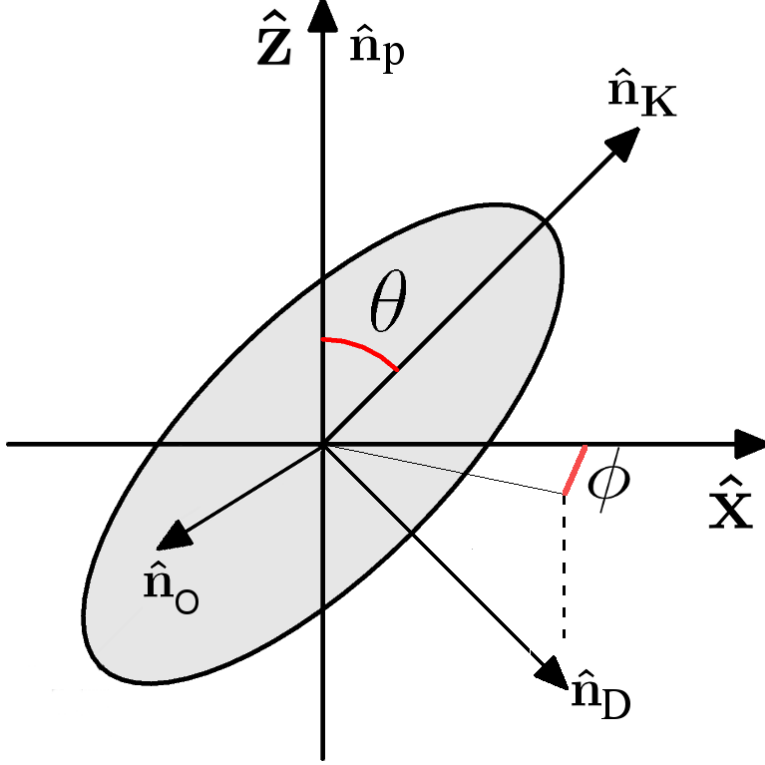


FIG. 1: Uniaxial and hard-axis anisotropy axes tilted with respect to polarizer by angle θ .

$p \equiv \hat{\mathbf{n}}_O \cdot \mathbf{m}$ of the magnetization vector along this new set of axes. Written componentwise, they are:

$$\dot{s} = qp - \alpha \left[(In_x \sqrt{1-n^2} + Ds)(1-s^2) + qs(In_z + q) + In_x n s p \right] \quad (8)$$

$$\dot{q} = Ds p + \alpha \left[(In_z + q)(1-q^2) + Iq n_x (s \sqrt{1-n^2} - np) + Ds^2 q \right] \quad (9)$$

$$\dot{p} = -(D+1)qs + \alpha \left[s p (In_x \sqrt{1-n^2} + Ds) - qp(In_z + q) + In_x n (1-p^2) \right]. \quad (10)$$

III. THERMAL EFFECTS

Thermal effects are included by considering uncorrelated fluctuations in the effective interaction field: $\mathbf{H}_{\text{eff}} \rightarrow \mathbf{H}_{\text{eff}} + \mathbf{H}_{th}$. These transform the LLG equation into its Langevin form. We model the stochastic contribution \mathbf{H}_{th} by specifying its correlation properties, namely:

$$\langle \mathbf{H}_{th} \rangle = 0 \quad (11)$$

$$\langle H_{th,i}(t)H_{th,k}(t') \rangle = 2C\delta_{i,k}\delta(t-t') \quad (12)$$

The effect of the random torque \mathbf{H}_{th} is to produce a diffusive random walk on the surface of the \mathbf{M} -sphere. An associated Fokker-Planck equation describing such dynamics was constructed by Brown⁶. At long times, the system attains thermal equilibrium; by the fluctuation-dissipation theorem we have

$$C = \frac{\alpha k_B T}{2K(1 + \alpha^2)} = \frac{\alpha}{2(1 + \alpha^2)\xi}, \quad (13)$$

where $\xi = K/k_B T$ is the barrier height due to the uniaxial anisotropy energy divided by the thermal energy.

Setting the external magnetic field to zero and considering only thermal fluctuations, the stochastic LLG equation reads:

$$\dot{m}_i = A_i(\mathbf{m}) + B_{ik}(\mathbf{m}) \circ H_{th,k} \quad (14)$$

where

$$\begin{aligned} \mathbf{A}(\mathbf{m}) &= \alpha I \left[\alpha \mathbf{m} \times \hat{\mathbf{k}} - \mathbf{m} \times (\mathbf{m} \times \hat{\mathbf{k}}) \right] \\ &\quad - (\hat{\mathbf{n}}_K \cdot \mathbf{m}) [\mathbf{m} \times \hat{\mathbf{n}}_K - \alpha (\hat{\mathbf{n}}_K - (\hat{\mathbf{n}}_K \cdot \mathbf{m})\mathbf{m})] \\ &\quad + D(\hat{\mathbf{n}}_D \cdot \mathbf{m}) [\mathbf{m} \times \hat{\mathbf{n}}_D - \alpha (\hat{\mathbf{n}}_D - (\hat{\mathbf{n}}_D \cdot \mathbf{m})\mathbf{m})], \end{aligned} \quad (15)$$

$$B_{ik}(\mathbf{m}) = -\epsilon_{ijk}m_j - \alpha(m_i m_k - \delta_{ik}). \quad (16)$$

and ‘ $\circ H_{th,k}$ ’ means that the multiplicative noise term in the dynamical equation is to be interpreted in the sense of Stratonovich calculus²⁵¹⁶.

We numerically solve the above Langevin equations by using a standard second-order Heun scheme to ensure proper convergence. At each time step, the strength of the random kicks is given by the fluctuation-dissipation theorem. Statistics were gathered from an ensemble of 5000 events with a natural integration stepsize of 0.01. For concreteness, we set the damping constant $\alpha = 0.04$ and the barrier height to $\xi = 80$. To explore the simulations for long time regimes, the necessary events were simulated in parallel on an NVidia Tesla

C2050 graphics card. To generate the large number of necessary random numbers, we chose a proven combination¹⁷ of the three-component combined Tausworthe “taus88”¹⁸ and the 32-bit “Quick and Dirty” LCG¹⁹. The hybrid generator provides an overall period of around 2^{121} .

IV. SWITCHING DYNAMICS

In experiments, one is generally interested in understanding how the interplay between thermal noise and spin torque effects switch an initial magnetic orientation from parallel to antiparallel. The role of spin torque from an energy landscape point of view can be elucidated by considering how energy is pumped into the system. As in the previous section, the monodomain’s magnetic energy (for $\mathbf{h} = 0$) can be written in dimensionless form:

$$\epsilon(\mathbf{m}) \equiv U(\mathbf{m})/K = D(\hat{\mathbf{n}}_D \cdot \mathbf{m})^2 - (\hat{\mathbf{n}}_K \cdot \mathbf{m})^2 = Ds^2 - q^2. \quad (17)$$

Stable states with minimum energy have $q = \pm 1$ and thus $\epsilon = -1$. The change in energy over time can then be written as:

$$\dot{\epsilon} = 2 [Ds\dot{s} - q\dot{q}]. \quad (18)$$

The dynamical equations (14) for \dot{s} and \dot{q} can be plugged back in to (17) to obtain a dynamical equation for the energy:

$$\dot{\epsilon} = f(s, q) + g(s, q) \circ \dot{W}. \quad (19)$$

Nanomagnets typically operate in a regime where the nonconservative parts of the dynamics, including the effects of damping, STT and thermal noise, act on timescales that are long compared to the energy-conserving piece of the Hamiltonian. Trajectories are therefore expected to remain close to periodic Hamiltonian orbits for a long time, slowly drifting from one orbit to another. Using this information, we average the energy evolution equation (19) over constant energy trajectories, thereby obtaining a diffusion equation in energy space^{11–13}. From (7) we have

$$\dot{s}^0 = -q^0 p^0 \quad (20)$$

$$\dot{q}^0 = -D s^0 p^0 \quad (21)$$

$$\dot{p}^0 = (D + 1) q^0 s^0, \quad (22)$$

the solutions of which can be expressed in terms of Jacobi elliptic functions:

$$s^0(t) = \mp \sqrt{D \frac{1+\epsilon}{D+1}} \operatorname{cn} \left[\sqrt{D-\epsilon} t, k^2 \right] \quad (23)$$

$$q^0(t) = \pm \sqrt{\frac{D-\epsilon}{D+1}} \operatorname{dn} \left[\sqrt{D-\epsilon} t, k^2 \right] \quad (24)$$

$$p^0(t) = -\sqrt{1+\epsilon} \operatorname{sn} \left[\sqrt{D-\epsilon} t, k^2 \right], \quad (25)$$

where $k^2 \equiv D \frac{1+\epsilon}{D-\epsilon}$. The period of these trajectories as a function of energy can be expressed as a complete elliptic integral of the first kind:

$$T(\epsilon) = \frac{4}{\sqrt{D-\epsilon}} \int_0^1 \frac{dx}{\sqrt{(1-x^2)(1-k^2 x^2)}} = \frac{4}{\sqrt{D-\epsilon}} \mathbf{K}(k^2). \quad (26)$$

A sample of these trajectories for energies greater and less than 0 are shown in Fig. 2. The $\epsilon < 0$ dynamics consist of the magnetization precessing around the uniaxial axis ($\hat{\mathbf{n}}_K$), thus remaining in the energy minimum's basin of attraction. On the other hand, for $\epsilon > 0$ the magnetization precesses around the hard axis ($\hat{\mathbf{n}}_D$). Magnetic switching, defined as a transition from one $\epsilon < 0$ basin to another, must proceed through an intermediate $\epsilon > 0$. As a result, we will consider $\epsilon = 0$ to be the critical threshold energy that a monodomain must surpass to achieve switching.

The qualitative properties of such trajectories are better understood by parametrizing them geometrically as follows. The energy landscape (17) determines the geometrical conditions these trajectories must satisfy. For $\epsilon > 0$ we have

$$\frac{D}{\epsilon} s^2 - \frac{1}{\epsilon} q^2 = 1 \quad (27)$$

$$s^2 + q^2 + p^2 = 1. \quad (28)$$

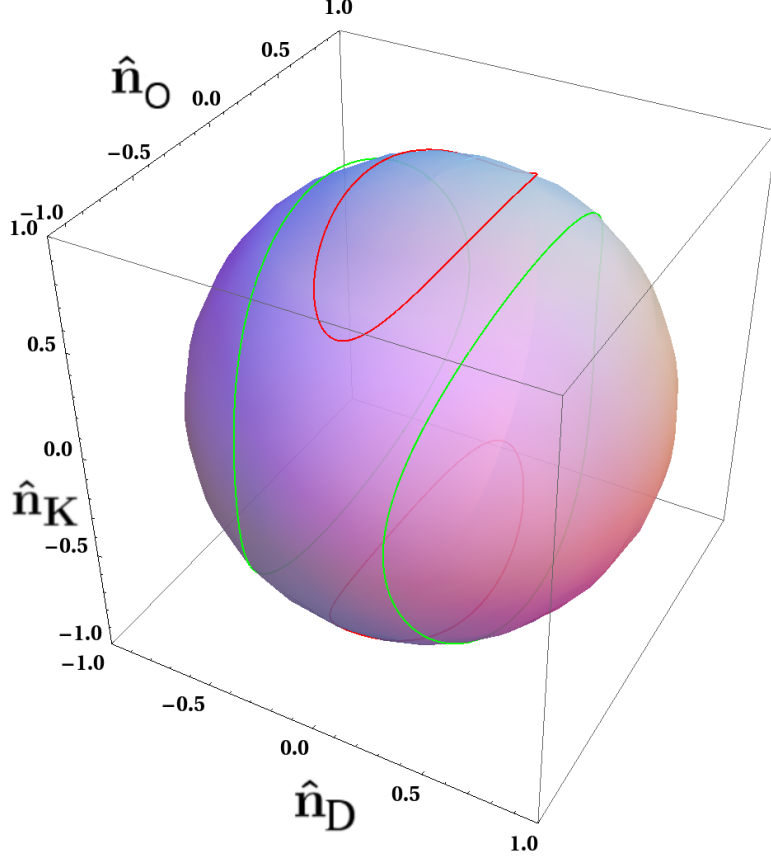


FIG. 2: Constant energy trajectories. $\epsilon < 0$ trajectories are shown in red whereas $\epsilon > 0$ trajectories are shown in green.

These are satisfied by the parametrization:

$$s^0(w) = \pm \sqrt{\frac{|\epsilon|}{D}} \cosh(w) \quad (29)$$

$$q^0(w) = \sqrt{|\epsilon|} \sinh(w) \quad (30)$$

$$p^0(w) = \pm \sqrt{1 + |\epsilon|} \sqrt{1 - \gamma_+^2 \cosh^2(w)}, \quad (31)$$

$$\gamma_+^2 = \frac{\epsilon(D+1)}{D(\epsilon+1)}. \quad (32)$$

where the limits of validity of $-\text{acosh}(1/\gamma_+) < w < \text{acosh}(1/\gamma_+)$ are found by imposing the extra condition that for $p = 0$, $s^2 + q^2 = 1$. The identical reasoning carried out for $\epsilon < 0$

leads to the parametrization:

$$s^0(w) = \pm \sqrt{\frac{|\epsilon|}{D}} \sinh(w) \quad (33)$$

$$q^0(w) = \pm \sqrt{|\epsilon|} \cosh(w) \quad (34)$$

$$p^0(w) = \pm \sqrt{\frac{D+|\epsilon|}{D}} \sqrt{1 - \gamma_-^2 \cosh^2(w)}, \quad (35)$$

$$\gamma_-^2 = \frac{|\epsilon|(D+1)}{D+|\epsilon|}, \quad (36)$$

with limits $-\text{acosh}(1/\gamma_-) < w < \text{acosh}(1/\gamma_-)$.

We are now ready to average (18) over constant energy orbits. The averaging procedure is simplified by noting that we are interested in switching behavior starting from the $\epsilon < 0$ basin and that in that basin the constant energy trajectories are symmetric with respect to the $\hat{\mathbf{n}}_K$ axis. As such, the majority of terms obtained by inserting (8) into (18) will average to zero. The remaining nonzero terms lead to the averaged energy equation:

$$\begin{aligned} \langle \partial_t \epsilon \rangle &= -2\alpha [In_z(1+\epsilon)\langle q \rangle + (1+\epsilon)\langle q^2 \rangle + D(D-\epsilon)\langle s^2 \rangle] \\ &+ 2\sqrt{\frac{\alpha(D+1)}{\xi}} \sqrt{\langle q^2 \rangle + \frac{D-\epsilon}{D+1}} \epsilon \circ \dot{W} \end{aligned} \quad (37)$$

where $\langle \cdot \rangle$ implies averaging over constant energy orbits as described. Construction of the stochastic term requires averaging the variance of (18) following the rules of additivity for Gaussian random variables. It is seen from (37) that the applied current factors into this equation only in the form In_z , where n_z is the cosine of the angular tilt between uniaxial anisotropy and polarizer axes. This leads to a more general form of a result obtained in our previous work⁸, namely that scalings between switching times and applied current will be functionally identical independent of the incoming angle of the spin-polarized current. The only caveat here is that every current must be rescaled by multiplying it by n_z . Analogously, the azimuthal tilt parameter n does not appear at all in the energy-averaged equation, implying that only coplanar setups between polarizer, easy and hard axes need to be considered in what follows.

With this understanding, we can now omit the notation n_z and consider macrospin setups with no angular tilt between polarizer and uniaxial anisotropy axes. The next step is to show how the necessary averages can be computed explicitly. As an example, consider $\langle q \rangle$; its average is given by:

$$\langle q \rangle = \frac{1}{T(\epsilon)} \int_0^T dt q^0(t), \quad (38)$$

where the integration is over time and one uses the expression for q^0 in terms of its Jacobi elliptic function. We can express the same integral in terms of the geometrical parametrization (33). In fact

$$\langle q \rangle = \frac{1}{T(\epsilon)} \int_0^T dt q^0(t) = \frac{1}{T(\epsilon)} \oint dw \frac{ds^0/dw}{\dot{s}^0} q^0(w). \quad (39)$$

Putting together the expression for \dot{s}^0 from (20) and, again, employing the geometrical parametrizations from (33), we obtain

$$\langle q \rangle = -\frac{4}{T(\epsilon)\sqrt{D+1}} \int_0^{\text{acosh}(1/\gamma)} dw \frac{\cosh(w)}{\sqrt{1-\gamma^2 \cosh^2(w)}} = -\frac{2\pi}{T(\epsilon)\sqrt{D+1}}, \quad (40)$$

where, for notational convenience, we redefine $\gamma = \gamma_-$.

Repeating the procedure for the other terms in (8), we write

$$\langle q^2 \rangle(\epsilon) = \frac{4}{T(\epsilon)\sqrt{D+1}} \sqrt{\frac{D}{D+1-\gamma^2}} \eta_1 \quad (41)$$

$$\langle s^2 \rangle(\epsilon) = \frac{4}{T(\epsilon)\sqrt{D+1}} \sqrt{\frac{D}{D+1-\gamma^2}} \frac{1}{D} (\eta_1 - \gamma^2 \eta_0), \quad (42)$$

with

$$\eta_0(\epsilon) = \int_0^1 \frac{dx}{\sqrt{(\gamma^2 + (1-\gamma^2)x^2)(1-x^2)}} = \frac{K(1-\frac{1}{\gamma^2})}{\gamma} = K(1-\gamma^2) \quad (43)$$

$$\eta_1(\epsilon) = \int_0^1 dx \sqrt{\frac{\gamma^2 + (1-\gamma^2)x^2}{1-x^2}} = \gamma E(1-\frac{1}{\gamma^2}) = E(1-\gamma^2) \quad (44)$$

$$T(\epsilon) = 4\sqrt{\frac{D+1-\gamma^2}{D(D+1)}} K(1-\gamma^2) = 4\sqrt{\frac{D+1-\gamma^2}{D(D+1)}} \eta_0(\gamma) \quad (45)$$

$$\gamma(\epsilon) = \frac{|\epsilon|(D+1)}{D+|\epsilon|}, \quad (46)$$

where $K(x)$ and $E(x)$ are elliptic functions of the first and second kind respectively (Appendix A). The energy equation for the dynamics starting in the negative energy well ($0 < |\epsilon| < 1$) then reads (expressed in terms of γ^{26}):

$$\begin{aligned} \partial_t |\epsilon|(\gamma) &= \frac{8\alpha}{T(\gamma)} \left(\frac{D(D+1)^{1/3}}{D+1-\gamma^2} \right)^{3/2} \left[\eta_1(\gamma) - \gamma^2 \eta_0(\gamma) + \frac{1-\gamma^2}{D} \left(\eta_1(\gamma) - \frac{\pi I}{2} \sqrt{\frac{D+1-\gamma^2}{D}} \right) \right] \\ &+ 4\sqrt{\frac{\alpha}{\xi T(\gamma)}} \left(\frac{D(D+1)}{D+1-\gamma^2} \right)^{1/4} \sqrt{\eta_1(\gamma) - \frac{D\gamma^2}{D+1-\gamma^2} \eta_0(\gamma)} \circ \dot{W}. \end{aligned} \quad (47)$$

In outlining the steps above, we have succeeded in reducing the multidimensional complexity of the full magnetization dynamics to a one-dimensional stochastic differential equation whose properties we now proceed to study. The relation to previous studies^{8,9} on uniaxial macrospins can be rederived by considering equations (20) and (47) in the limit $D \rightarrow 0$. Doing so leads to the much simplified energy diffusion equation¹⁵

$$\partial_t |\epsilon| = 2\alpha \sqrt{|\epsilon|} (1 - |\epsilon|) (\sqrt{|\epsilon|} - I) + 2\sqrt{\frac{\alpha}{\xi}} |\epsilon| (1 - |\epsilon|) \circ \dot{W}, \quad (48)$$

with a stable energy minimum at $\epsilon = -1$ and saddle point at $\epsilon = -I^2$. This equation also shows that, for currents $I > I_c = \max_{|\epsilon| \in [0,1]} \sqrt{|\epsilon|} = 1$, the flow becomes negative for all values of $|\epsilon|$, so that in this regime all states will deterministically switch.

V. STABILITY ANALYSIS

In the absence of applied currents, $\partial_t |\epsilon| > 0$ as determined by (47) and ϵ flows toward its minimum value of -1 (the stable fixed point of its dynamics). To understand switching one must therefore investigate under what circumstances ϵ may become greater than zero, thus implying a transition from the red to the green trajectories discussed in Fig. 2. It suffices to understand the behavior of the energy flow at the stable fixed point of the zero current dynamics ($|\epsilon| = \gamma = 1$) and at the energy threshold for switching ($|\epsilon| = \gamma = 0$). These limiting flows are found by computing the integrals $\eta_0(\gamma)$ and $\eta_1(\gamma)$. One finds:

$$\lim_{\gamma \rightarrow 1} \eta_0(\gamma) \sim \frac{\pi}{2} + \frac{\pi}{8} \frac{D}{D+1-\gamma^2} (1 - \gamma^2) + o((1 - \gamma^2)^2) \quad (49)$$

$$\lim_{\gamma \rightarrow 1} \eta_1(\gamma) \sim \frac{\pi}{2} - \frac{\pi}{8} \frac{D}{D+1-\gamma^2} (1 - \gamma^2) + o((1 - \gamma^2)^2), \quad (50)$$

and

$$\lim_{\gamma \rightarrow 0} \eta_0(\gamma) \sim \log(\gamma) + o(\log(\gamma)\gamma^2) \quad (51)$$

$$\lim_{\gamma \rightarrow 0} \eta_1(\gamma) \sim 1 + o(\gamma). \quad (52)$$

Using these results in (47), one finds that in the absence of thermal noise (i.e., the zero temperature limit), the limiting flows are:

$$\lim_{\gamma \rightarrow 0} \partial_t |\epsilon| = \frac{8\alpha}{T} \frac{\sqrt{D}}{D+1} \left[D + 1 - \frac{\pi I}{2} \sqrt{\frac{D+1}{D}} \right] \quad (53)$$

$$\lim_{\gamma \rightarrow 1} \partial_t |\epsilon| = \frac{4\pi\alpha}{T} \frac{\sqrt{D+1}}{D} (1 - \gamma^2) [D + 2 - 2I]. \quad (54)$$

As expected, both eqs. (53) and (54) show how the qualitative behavior of the deterministic energy flow can be tuned by the value of applied current. The stability of the zero current stable fixed point ($|\epsilon| = \gamma = 1$) can in fact be rendered unstable once (54) changes sign at the applied current value:

$$I_c^{|\epsilon|=1} \equiv I_C^1 = \frac{D + 2}{2}. \quad (55)$$

Analogously, at $|\epsilon| = \gamma = 0$ the flow is either positive or negative depending on the applied current. Using (53), we find that the sign of the flow switches from positive to negative at

$$I_c^{|\epsilon|=0} \equiv I_C^0 = \frac{2}{\pi} \sqrt{D(D+1)}. \quad (56)$$

Identical expressions for the critical currents have recently been derived by Taniguchi¹⁴ via different means. These two critical stability thresholds are identical at a critical value of D :

$$D_0 = 2 \frac{\pi^2 - 4}{16 - \pi^2} \left[1 + 2 \frac{\sqrt{4 + 2\pi^2}}{\pi^2 - 4} \right] \sim 5.09. \quad (57)$$

The value of D relative to D_0 , as well as the applied current, will select between two qualitatively different dynamical regimes. We now proceed to explore both.

A. $D > D_0$

When the ratio between hard and easy axis anisotropies is greater than the threshold value D_0 , $I_C^0 > I_C^1$ (see Fig. 3). Unless the applied current is greater than I_C^0 , deterministic switching of the monodomain cannot be achieved. This differs from conclusions drawn by previous work²⁰ where the critical current for deterministic switching was assumed to be that which renders the stable fixed point ($|\epsilon| = \gamma = 1$) unstable.

For small currents such that $I < I_C^1$, on the other hand, the deterministic flow pushes the energy toward the zero current stable fixed point. In such a scenario, switching can only occur via thermal activation over the $|\epsilon| = \gamma = 0$ effective barrier.

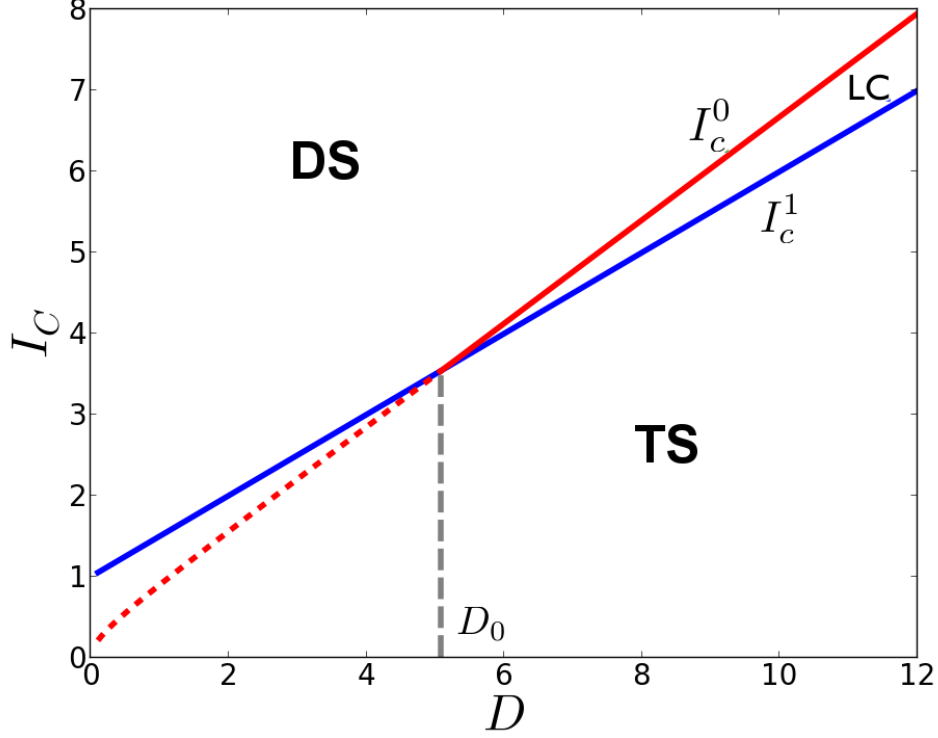


FIG. 3: Critical currents versus the ratio of the hard and easy axis anisotropies D . The blue curve is I_C^1 and the red curve is I_C^0 . For $D < D_0$, currents greater than I_C^1 lead to deterministic switching (labeled DS). For $D > D_0$ currents between I_C^0 and I_C^1 lead to limit cycles (LC). Limit cycles can also occur for currents just below and approximately equal to I_C^1 for $D < D_0$, as shown in Fig. 7

Finally, for currents $I_C^0 > I > I_C^1$, the zero current stable fixed point has been rendered unstable while the flow at the switching energy threshold remains positive. The monodomain will move (deterministically) from the $|\epsilon| = \gamma = 1$ fixed point, but switching over the $|\epsilon| = \gamma = 0$ must still take place via thermal activation. This implies that a new stable energy equilibrium exists for some value $0 < \tilde{\gamma}_S < 1$. The precessional macrospin dynamics will then manifest itself in the form of stable limit cycles. This has been observed both experimentally²¹ and numerically¹¹. These three dynamical scenarios are displayed in Fig. 4 where the deterministic energy flow is plotted as a function of energy.

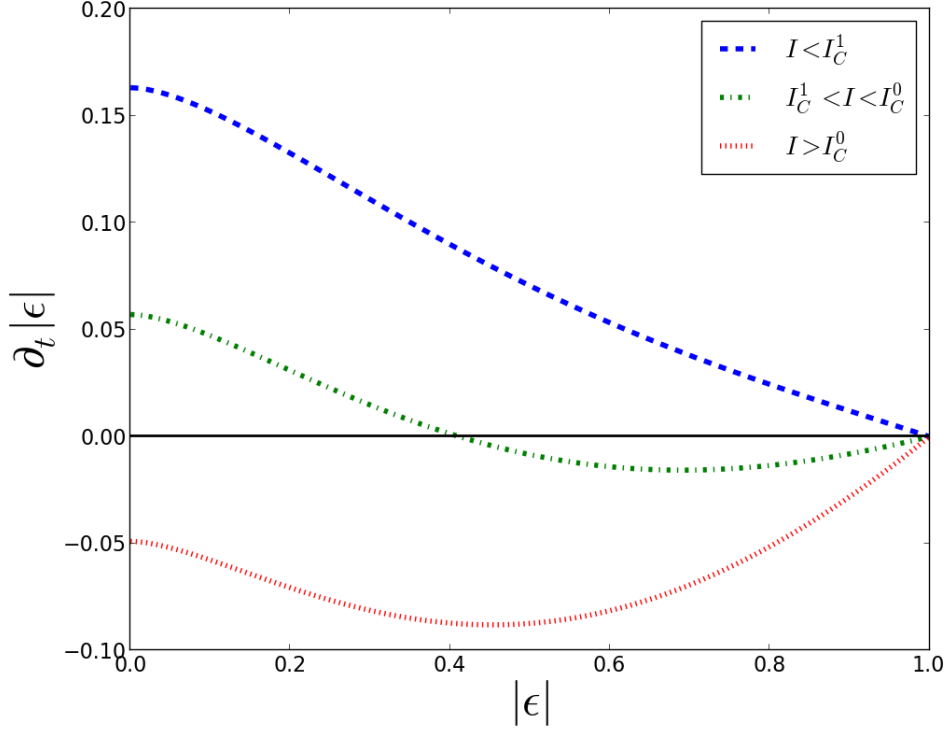


FIG. 4: Three sample regimes of deterministic energy flow $\dot{\epsilon}$ as a function of energy for $D > D_0$. Coloring (online) is included to better distinguish the various curves. a) $I < I_C^1$: Subcritical regime, thermal noise must oppose a positive energy flow to achieve switching; b) $I_C^1 < I < I_C^0$: Limit cycle regime; and c) $I > I_C^0$: Supercritical regime, negative flow leads to determinist switching.

B. $D < D_0$

When the ratio between hard and easy axis anisotropies is smaller than the threshold value D_0 , we have $I_C^1 > I_C^0$ (see Fig 3). The threshold critical current that switches all magnetic states deterministically is now I_C^{120} . Above this value of the applied current, switching will occur independently of thermal noise effects.

For applied currents such that $I_C^0 < I < I_C^1$, a saddle point emerges for some value $0 < \tilde{\gamma}_U < 1$. For switching to occur, thermal activation must move the monodomain energy past this saddle point. As the current is lowered, $\tilde{\gamma}_U$ becomes progressively smaller until the limiting value $\tilde{\gamma}_U = 0$. At this point, switching requires thermal activation throughout the whole energy range. These three dynamical scenarios are displayed in Fig. 5 where the

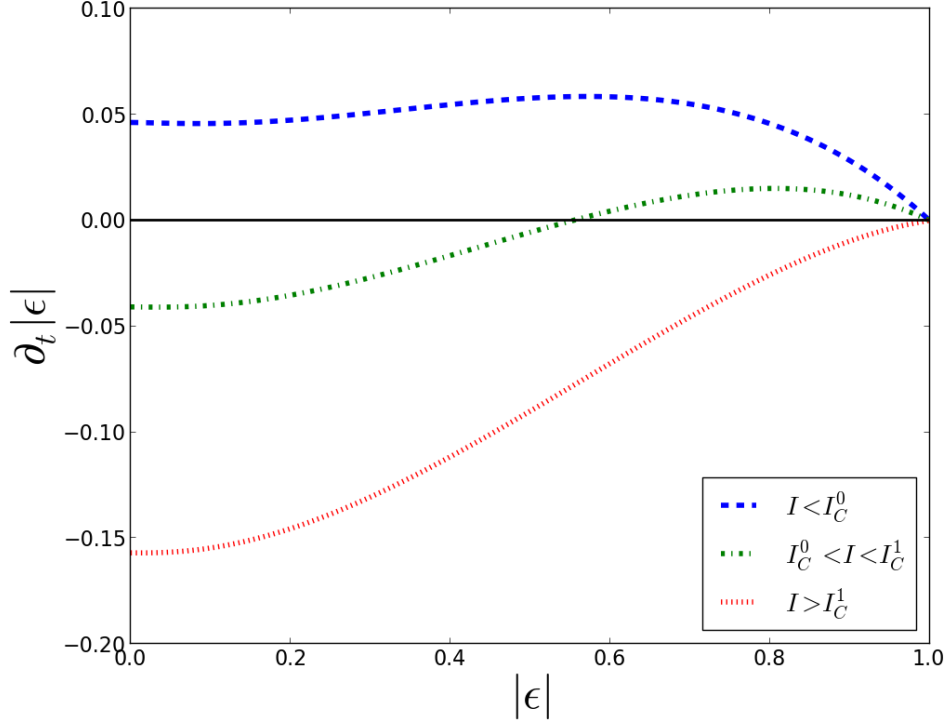


FIG. 5: Three sample regimes of deterministic energy flow $\dot{\epsilon}$ as a function of energy for $D < D_0$. Coloring (online) is included to better distinguish the various curves. a) $I < I_C^0$: Subcritical regime, thermal noise must oppose a positive energy flow to achieve switching; b) $I_C^0 < I < I_C^1$: Crossover regime, switching is still achieved via thermal activation but the unstable equilibrium has now shifted; and c) $I > I_C^1$: Supercritical regime, negative flow leads to determinist switching.

deterministic energy flow is plotted as a function of energy.

It is interesting to note that the condition $D < D_0$ can also result in the appearance of limit cycles. Limit cycle regimes in fact can be seen for very small applied ranges of current less than I_C^0 (Fig. 6).

The uniaxial macropin model is a particular case of a $D < D_0$ model ($D = 0$). By taking the limit $D \rightarrow 0$, we find $I_C^0 \rightarrow 0$ and $I_C^1 \rightarrow 1$, as found in previous work.⁸ For all values of the applied current strictly between 0 and 1, uniaxial macropin switching must take place via thermal activation over an effective energy barrier.

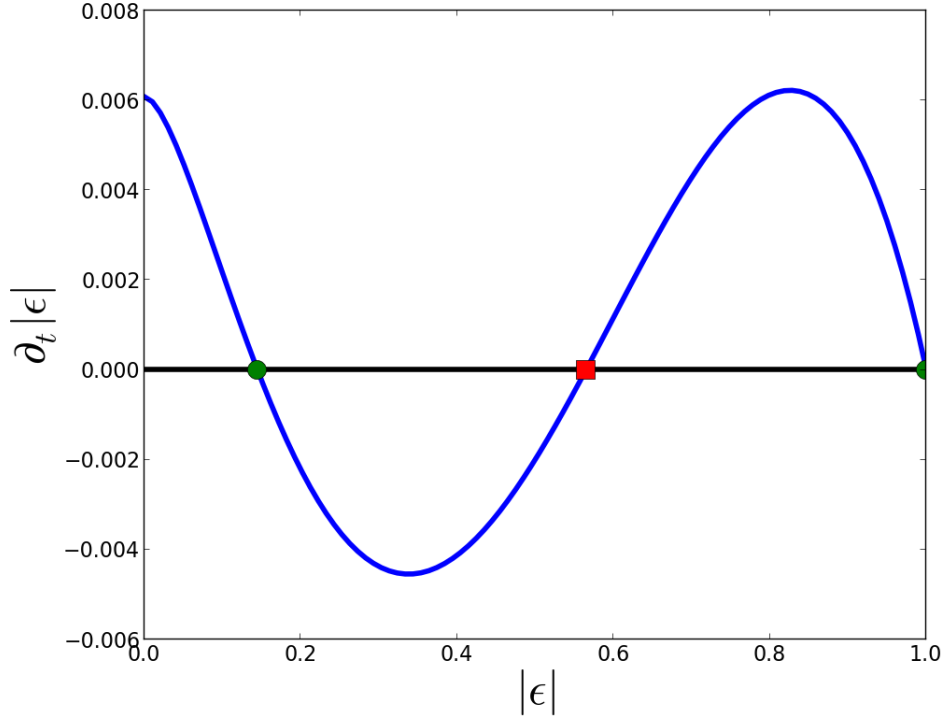


FIG. 6: Energy flow for a $D = 4$ macrospin and applied current $I = 2.82 < I_C^0$. Circles and squares respectively represent stable and unstable equilibria. For these parameters ($D = 4$ and $I = 2.82$), two stable equilibria of the zero temperature dynamics coexist.

VI. LIMITS OF THE CEOA APPROACH

In this section we will determine under what conditions the CEOA approach is valid. The fundamental assumption is that the deterministic precession timescale of the constant energy orbits be small compared to the timescale over which significant energy diffusion due to noise and spin-torque transfer takes place. We now quantify this condition and obtain precise limits in terms of the applied current intensity I and the anisotropy ratio D . For our approximations to be valid, the averaged energy flow ($T(\epsilon)\partial_t|\epsilon|$) over any given orbit must be small compared to the maximum allowable energy ($0 < |\epsilon| < 1$):

$$\max_{\epsilon} T(\epsilon)|\partial_t|\epsilon|| = \max_{\gamma} T(\gamma)|\partial_t|\epsilon|| \ll 1, \quad (58)$$

where we continue to use the variable $\gamma(\epsilon) = |\epsilon|(D+1)/(D+|\epsilon|)$. To proceed, we consider the deterministic drift and random components of the energy flow separately. Noise averag-

ing (47) will give the contribution of the drift to the energy flow. The intensity of the orbit averaged drift then reads:

$$T(\gamma)|\langle\partial_t|\epsilon|\rangle| = 8\alpha \left(\frac{D(D+1)^{1/3}}{D+1-\gamma^2}\right)^{3/2} \left| \eta_1(\gamma) - \gamma^2\eta_0(\gamma) + \frac{1-\gamma^2}{D} \left(\eta_1(\gamma) - \frac{\pi I}{2} \sqrt{\frac{D+1-\gamma^2}{D}} \right) \right|, \quad (59)$$

where angular brackets denote noise averaging. This expression can be shown to be finite for all values of γ , I and D . Furthermore, for applied currents greater than I_C^0 , (59) has a maximum at $\gamma = 0$; its value in this limit is given by (53). Enforcing the conditions for validity discussed above results in an upper bound for the current:

$$I \ll \left(1 + \frac{1}{8\alpha\sqrt{D}}\right) I_C^0 \equiv I_M. \quad (60)$$

In the limit $D \rightarrow 0$, this expression converges to the correct uniaxial limit inequality $I \ll (4\pi\alpha)^{-1}$, discussed previously in¹⁵.

When switching occurs deterministically (and $I > I_C^0$), this bound is the sole limit to the validity of the CEOA approximation. This is because random contributions to the energy flow dynamics have zero mean. However, in scenarios where switching occurs due to thermal activation, one must consider the standard deviation of random contributions to the energy flow. These determine the rate of the rare events that drive the system over its confining energy barrier. The energy flow's standard deviation is $\sqrt{\langle[\partial_t|\epsilon| - \langle\partial_t|\epsilon|\rangle]^2\rangle}$. The orbit-averaged rate of random events driving noise-induced energy diffusion can then be written as:

$$T(\gamma)\sqrt{\langle[\partial_t|\epsilon| - \langle\partial_t|\epsilon|\rangle]^2\rangle} = 8\sqrt{\frac{\alpha}{\xi}\eta_0(\gamma) \left(\eta_1(\gamma) - \frac{D\gamma^2}{D+1-\gamma^2}\eta_0(\gamma) \right)}, \quad (61)$$

which can be shown to be both a monotonically decreasing function of γ and logarithmically divergent for $\gamma \rightarrow 0$. The latter is due to the limiting behavior of $\eta_0(\gamma)$ (see (51)) for all $D > 0$. The physical origin of this behavior lies in the divergence of the constant energy precessional period as the zero energy switching threshold is reached (a fact also pointed out by Taniguchi et al.¹⁴).

The relevant maxima of (61) will be located at the energy flow's saddle point γ_U . Unfortunately, solving for γ_U while imposing that the RHS of (61) be much less than 1 results in a set of transcendental equations which can only be solved numerically. However, we can set a precise bound by requiring that the saddle point never be at $\gamma_U = 0$ (where (61) diverges

for all $D > 0$). The applied current at which such a saddle point occurs has already been derived in (56), leading us to the lower bound inequality

$$I \gg I_C^0. \quad (62)$$

as the validity condition for CEOA in thermally activated scenarios. The reason for limiting ourselves to applied currents greater than I_C^0 in deriving the upper bound condition (60) is now justified.

As a result of (62), there are only two scenarios in which thermally activated switching can be analyzed and understood using CEOA dynamics. The first is in the limit $D \rightarrow 0$ (the uniaxial macrospin limit) where one has $\gamma(\epsilon) \rightarrow 1$ independently of ϵ . Divergences in the intensity of random contributions are then avoided for all ϵ and (61) takes the simple form $4\pi\sqrt{(\alpha/\xi)(1-\epsilon)}$. At $\epsilon = 0$ it converges to the finite value $4\pi\sqrt{\alpha/\xi}$ (which may still be large, however, depending on the ratio α/ξ). The second scenario is for models with $D < D_0$ and applied current values $I > I_C^0$. In these, the saddle point to be reached via thermal activation shifts to nonzero values $\gamma_U \neq 0$ where (61) does not diverge and the validity condition may be satisfied.

The above discussion demonstrates that thermally activated switching between dynamical limit cycle equilibria cannot be modeled with our technique. Thermal switching from a limit cycle, in fact, must proceed via noise diffusion up to a saddle point of the type $\gamma_U = 0$ where noise contributions diverge. Nonetheless, it should be noted that this does not necessarily invalidate the conditions for their existence discussed in the previous section. In fact, relaxation to a limit cycle is a drift-driven process for which noise related contributions average to zero. Our analysis merely shows that, once the macrospin has relaxed to its limit cycle state, further dynamics must proceed via thermal activation for which CEOA does not provide a suitable description.

In Fig. 7, the dynamical behavior for $D = 4$ is displayed. Here $D < D_0$ and $I_C^0 < I_C^1$. Fig. 7a shows the dependence between rescaled current and mean switching time for different polar angular tilts θ and fixed azimuthal angle ϕ . For reference, the critical currents I_C^0 , I_C^1 and I_C^M are shown. For large applied currents, deviations between the different sets of data are clearly visible. This discrepancy decreases as the current is lowered.

However, for $I < I_C^0$, the procedure is expected to fail due to the previously discussed divergence of the orbital period. To show this, we calculate the maximum deviation of

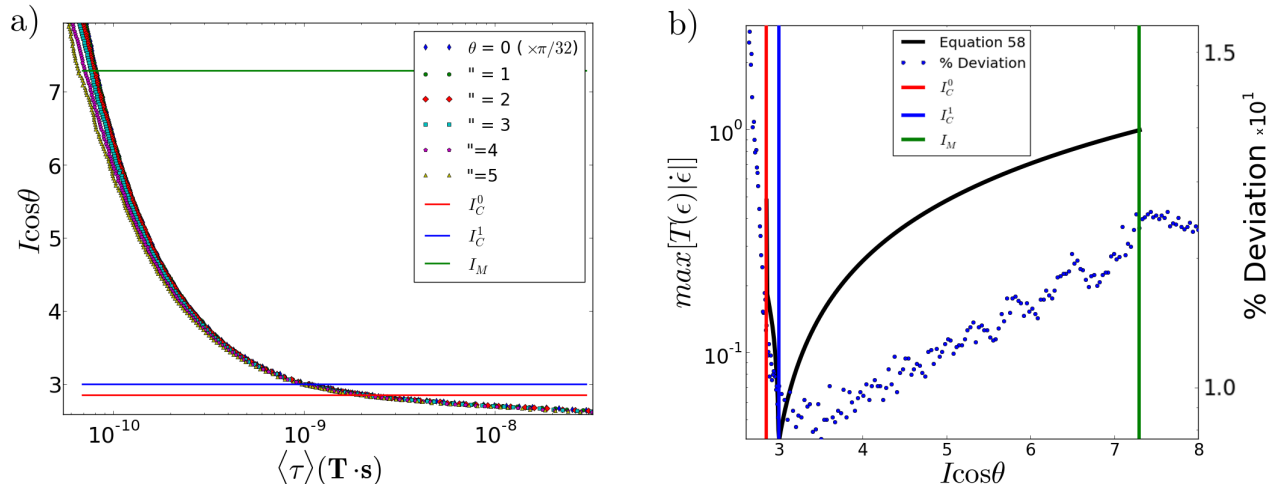


FIG. 7: **a)** Mean switching time versus current for $D = 4$, $\alpha = 0.04$ and $\xi = 80$ at different θ angular tilts with $\phi = 0$ kept fixed. All currents have been rescaled by $1/\cos\theta$. Times are shown in units of $(s \cdot T)$ where T stands for Tesla: real time is obtained upon division by H_K . For visual guidance, the critical currents I_C^0 and I_C^1 have been included. In a regime where the CEOA technique is applicable, the switching data from the various angular configurations should all fall on top of each other. **b)** Double axis plot of $\max[T(\epsilon)|\partial_t|\epsilon|]$ and the percent deviation of data from **(a)** as a function of normalized current. In the current range where the deterministic flow achieves its minimum, the deviation of the data does also. As the critical current I_C^0 is approached, deviation spikes are observed analogously to what can be inferred by the theory.

the mean switching time between all the angular data points at each value of the rescaled current (see Fig. 7b). As a further test, we have also numerically computed the LHS of (58) and compared it to the angular deviations. The critical currents I_C^0 , I_C^1 and I_C^M are again shown for reference. The theory is in satisfactory agreement with numerical simulations as can be seen from both the good alignment of the deviation minimum with the minimum of the maximum flow and the rapid spike in deviation as I_C^0 is approached.

This discussion implies that the CEOA technique applies best to small D macrospin models, and becomes increasingly inaccurate for larger D . Figs. 8 and 9 show the same analysis of a macrospin with $D = 50$ and one with $D = 7$. Fig. 8a indicates that the technique is not applicable for sufficiently high values of D . Nonetheless, theory and experiment approach each other near the minimum of the deterministic flow, as seen in Fig. 8b. As in Fig. 7, as currents drop below I_C^0 , deviations in the data rapidly spike.

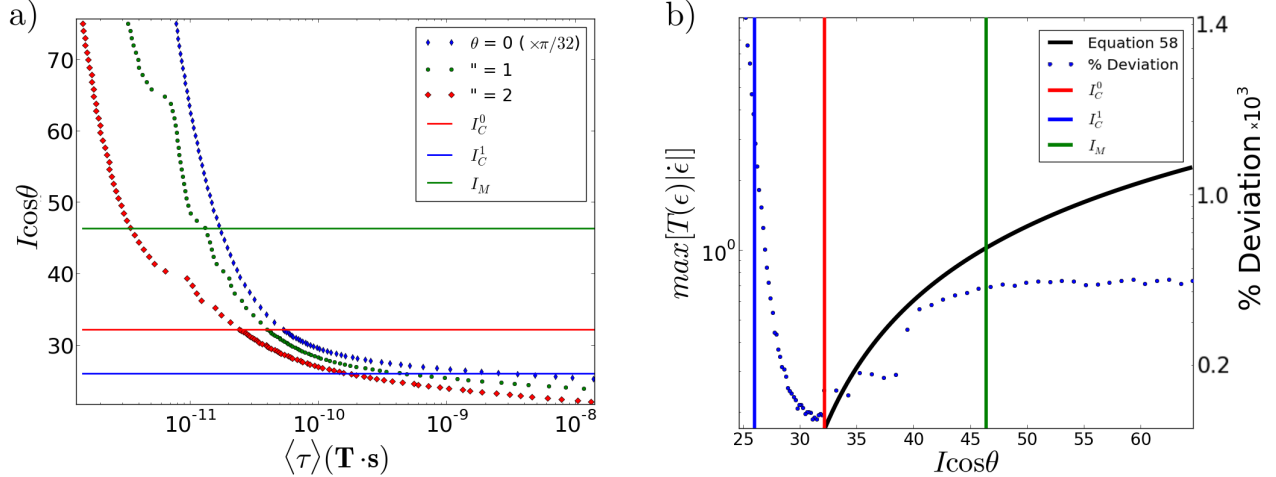


FIG. 8: **a)** Mean switching time versus current for $D = 50$, $\alpha = 0.04$ and $\xi = 80$ at different θ angular tilts with $\phi = 0$ kept fixed. All currents have been rescaled by $1/\cos\theta$. Times are shown in units of $(s \cdot T)$ where T stands for Tesla: real time is obtained upon division by H_K . For visual guidance, the critical currents I_C^0 and I_C^1 have been included. **b)** Double axis plot of $\max[T(\epsilon)|\partial_t|\epsilon|]$ and the percent deviation of data from **(a)** as a function of normalized current. In the current range where the deterministic flow achieves its minimum, the deviation of the data does also. As the critical current I_C^0 is approached, deviation spikes are observed analogously to what can be inferred by the theory.

The analysis and its comparison to numerical data indicate that the CEOA technique is best suited for studying macrospin dynamics in the crossover regime separating ballistic from fully activated thermal switching. Furthermore, the stability analysis of the energy dynamics (47) manages to capture the emergence of limit cycles even though it fails to describe thermally activated processes proceeding from them.

VII. THERMALLY ACTIVATED SWITCHING

Scenarios in which thermally activated switching can be studied using the approach described above are generally rather limited. Nonetheless, in the previous section, the technique was shown to be applicable in models with $D < D_0$ for currents $I_C^0 < I < I_C^1$. Starting from (47) one could in principle construct a Fokker-Planck equation describing energy diffusion and then attempt to solve an appropriate mean first passage time problem numerically.

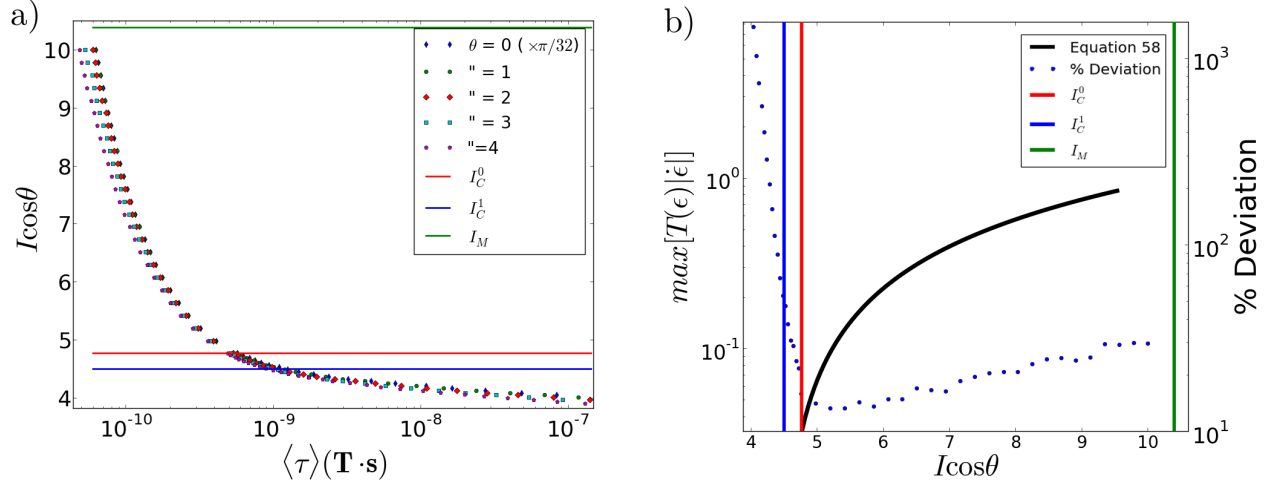


FIG. 9: **a)** Mean switching time versus current for $D = 7$, $\alpha = 0.04$ and $\xi = 80$ at different θ angular tilts with $\phi = 0$ kept fixed. All currents have been rescaled by $n_z = 1/\cos\theta$. Times are shown in units of $(s \cdot T)$ where T stands for Tesla: real time is obtained upon division by H_K . For visual guidance, the critical currents I_C^0 and I_C^1 have been included. **b)** Double axis plot of $\max[T(\epsilon)|\partial_t|\epsilon|]$ and the percent deviation of data from **(a)** as a function of normalized current. In the current range where the deterministic flow achieves its minimum, the deviation of the data does also. As the critical current I_C^0 is approached, deviation spikes are observed analogously to what can be inferred by the theory.

Instead, we will simplify the thermal activation problem by deriving the exponential scaling dependence between mean switching time and current, using an analytical tool described in¹⁵. In that paper, it was shown how, starting from energy diffusion dynamics analogous to (47), the exponential scaling dependence can be written in terms of an integral from the initial stable state to the saddle using a Friedlin-Wentzell²² type formulation:

$$\log(\langle \tau \rangle) \propto 2 \int_{|\epsilon_U|}^1 \frac{f(\epsilon')}{g^2(\epsilon')} d\epsilon' \quad (63)$$

where $f(\epsilon)$ and $g(\epsilon)$ are, respectively, the drift and noise terms of (47), now expressed in terms of the energy ϵ . This integral can be computed numerically once the saddle point of the energy flow has been identified (e.g. via a Newton algorithm). The integrand can be further expanded for $D \gg 1$ and approximated around the stable point $|\epsilon| = 1$. This gives,

to first order in $1 - |\epsilon|$,

$$\log(\langle\tau\rangle) \propto \xi \int_{|\epsilon v|}^1 \left(1 - (I/I_C^0) \sqrt{\frac{D}{D + \epsilon'}} \left(\frac{1 - \epsilon'}{\eta_1(\epsilon') - \epsilon' \eta_0(\epsilon')} \right) \right) d\epsilon' \quad (64)$$

$$\simeq \xi \int_{|\epsilon v|}^1 \left(1 - (I/I_C^0) \frac{1 - \epsilon'}{1 - \epsilon' \zeta(D)} \right) d\epsilon' \quad (65)$$

where $\zeta(D)$ is given by

$$\zeta(D) = \frac{I_C^1}{I_C^0} = \frac{\pi}{4} \left(\frac{D + 2}{\sqrt{D(D + 1)}} \right). \quad (66)$$

The approximated integral can now be written in closed form in terms of hypergeometric functions. The resulting expression is accurate to within 2% for values $D > 0.1$.

In Fig. 10 we plot the dependence of the mean switching time as a function of applied current, and compare it to $\log(\tau) \propto \xi(1 - I/I_C)^\beta$. In the limit $D \rightarrow 0$, the uniaxial switching exponent $\beta = 2$ is recovered. For larger values of D , the exponent β depends non-linearly on the applied current I . In the limit $I \rightarrow 0$ the limiting value of β can be derived analytically:

$$\lim_{I \rightarrow 0} \beta(I) = \lim_{I \rightarrow 0} \frac{\log(1 - \frac{q(D)}{I_C^0} I)}{\log(1 - I/I_C^1)} = q(D) \frac{I_C^1}{I_C^0}, \quad (67)$$

with

$$q(D) \equiv \int_0^1 \sqrt{\frac{D}{D + x}} \left(\frac{1 - x}{\eta_1(x) - x \eta_0(x)} \right) dx. \quad (68)$$

The same calculation can be performed in the limit $I \rightarrow I_C^1$ and used to show that the exponent β diverges for all non-zero values of D . The mean switching time is nonetheless well behaved, as can be seen in Fig. 10a. This differs from the results obtained by Taniguchi¹⁴, in which the limiting value of the exponent β is roughly 2.2, as the applied current approaches the critical threshold for deterministic switching.

VIII. CONCLUSION

This paper extends the analytical approach introduced by the authors in¹⁵ and applies it to the biaxial macrospin model. We have described a technique that reduces the complexity of the 3D macrospin reversal dynamics, under the action of both spin-torque and thermal noise, to a 1D stochastic equation in the energy space of the macrospin. To do so, the complete macrospin dynamics were approximated over precessional constant energy orbits.

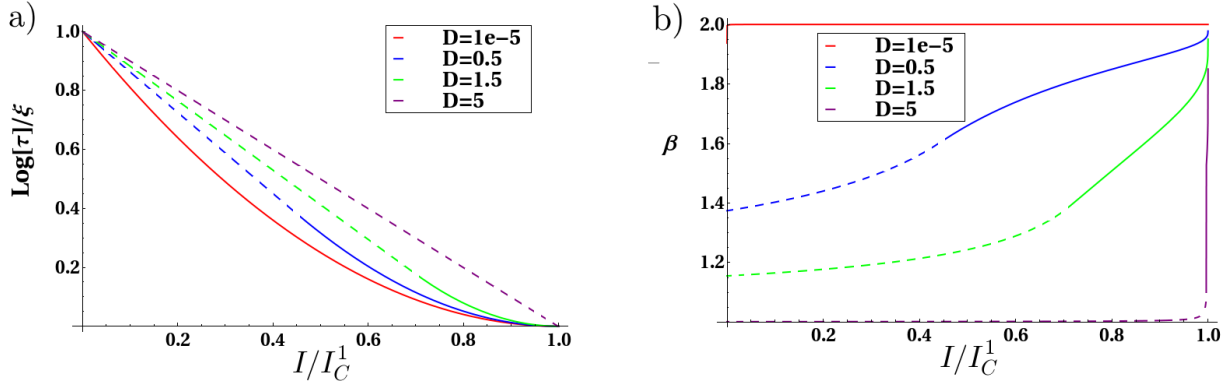


FIG. 10: **a)** Scaling dependence of mean switching time as a function of applied current I for models with varying $D < D_0$. ξ is the energy barrier height and I_C^1 the critical current threshold for deterministic switching. **b)** Fit of (64) to the form $(1 - I/I_C^1)^\beta$. Dashed lines represent continuation of analytical results outside the technique's regime of validity. Fitting exponent β is plotted as a function of applied current for models with varying D . In the limit of small D the exponent approaches the constant value $\beta = 2$ consistent with previous uniaxial macrospin results^{8,10,15}. For $D > 0$, the exponent β depends nonlinearly on the applied current intensity. Only for values $D \sim D_0$ do we notice that in the limit of small applied currents, $\beta \rightarrow 1$ as suggested by similar energy diffusion studies from the literature^{11,12}. For intermediate values $D_0 > D > 0$ the low current limit of β can be obtained analytically (67). On the other hand, in the limit $I \rightarrow I_C^1$ the exponent β can be shown to diverge for all non-zero values of D .

Under such an approximation, the resulting theory predicts that the geometries involved influence the respective dynamics in very precise ways. We found that the angular tilt between spin polarization and uniaxial anisotropy axes factors into the dynamics only as a trivial rescaling of the applied current. Similarly, the relative orientation of the hard axis is predicted to play no role in the switching dynamics under conditions in which constant-energy orbit averaging (CEOA) is a valid assumption.

The main parameter characterizing the different dynamical regimes is the ratio D between the hard and easy axis anisotropies. For a specific value of D , two critical currents ($I_C^1 = (D + 2)/2$, $I_C^0 = (2/\pi)\sqrt{D(D + 1)}$) are found to exist. The relative magnitude of these critical currents depends nonlinearly on D . For $D > D_0 \simeq 5.09$, we showed that stable limit cycle magnetization precessions appear in well-defined current ranges; transitions between these stable limit cycles proceeds through thermal activation. When $D < D_0$, limit cycles

generally do not appear and the switching dynamics become qualitatively similar to those of a uniaxial macrospin model.

The CEOA procedure requires that the energy diffusion due to spin torque and thermal noise take place on a timescale much larger than the conservative precessional timescale of the model. This allows us to establish general conditions for the validity of CEOA dynamics.

We test our findings numerically by solving the full macrospin evolution equations and analyzing their applied current vs. mean switching time curves for various angular configurations. Our techniques are found to be applicable in explaining ranges of applied currents such that: $I \gg I_C^0$ where any thermally activated process proceeds along nearly precessional trajectories, and $I/I_C^0 \ll 1 + 1/(8\alpha\sqrt{D})$ such that spin torque intensity is minimized along the deterministic flow. These conditions do not generally hold in large D models, but do for small D . In the limit $D \rightarrow 0$ we recover known results for the uniaxial macrospin model. Our technique also appears to be suitable for studying thermally activated switching in models with $D < D_0$.

Finally, Friedlin-Wentzell theory was employed to analytically study the exponential scaling dependence between mean switching time and applied current in thermally activated scenarios. The exact analytical scaling was reduced to quadratures and an analytical approximation was suggested. The resulting analytical scaling dependence to the standard form $\log(\tau) \propto \xi(1 - I/I_C)^{\beta}$ and the current dependence of the exponent β was studied.

The exponent β was found to depend nonlinearly on the applied current intensity, similar to¹⁴. In the uniaxial macrospin limit $D \rightarrow 0$, the constant $\beta = 2$ result was recovered. For $D \neq 0$, β was found to depend on both the applied current intensity and the precise value of D .

Acknowledgments

The authors would like to acknowledge A. MacFadyen and J. Z. Sun for useful discussions and comments leading to this paper. This research was supported by NSF-DMR-100657, NSF-DMR-1309202 and PHY0965015.

* Electronic address: daniele.pinna@nyu.edu

- ¹ J. Slonczewski, J. Magn. Magn. Mater. **159**, L1 (1996).
- ² J. A. Katine, F. J. Albert, and R. A. Buhrman, Phys. Rev. Lett. **84**, 31493152 (2000).
- ³ L. Berger, Phys. Rev. B **54**, 9353 (1996).
- ⁴ B. Özyilmaz, A. D. Kent, J. Z. Sun, M. J. Rooks, and R. H. Koch, Phys. Rev. Lett. **93**, 176604 (2004).
- ⁵ A. Brataas, A. D. Kent and H. Ohno, Nature Materials **11**, 372 (2012).
- ⁶ W. F. Brown, Phys. Rev. **135**, 5 (1963).
- ⁷ T. Taniguchi and H. Imamura, Phys. Rev. B **85**, 18440 (2012).
- ⁸ D. Pinna, Aditi Mitra, D. L. Stein and A. D. Kent, arXiv:1205.6509 (2012).
- ⁹ D. Pinna, D. L. Stein, and A. D. Kent, arXiv:1210.7675 (2012).
- ¹⁰ T. Taniguchi and H. Imamura, Phys. Rev. B **83**, 054432 (2011).
- ¹¹ K. Newhall and E. Vanden-Eijnden, arXiv:1210.6253 (2012).
- ¹² D. M. Apalkov and P. B. Visscher, Phys. Rev. B **72**, 180405R (2005).
- ¹³ G. Bertotti, I. Mayergoyz, and C. Serpico, *Nonlinear Magnetization Dynamics in Nanosystems* (Elsevier, Oxford, UK, 2009).
- ¹⁴ T. Taniguchi, Y. Utsumi, M. Marthaler, D. S. Golubev and H. Imamura, Phys. Rev. B **87**, 054406 (2013).
- ¹⁵ D. Pinna, D. L. Stein, and A. D. Kent, arXiv:1210.7682 (2012).
- ¹⁶ I. Karatsas and S. Shreve, *Brownian Motion and Stochastic Calculus, 2nd ed.* (Springer-Verlag, New York, 1997).
- ¹⁷ H. Nguyen, *GPU Gems 3* (Addison-Wesley Professional, 2007).
- ¹⁸ P. L'Ecuyer, Operations Research **44**, 5 (1996), pp. 816-822.
- ¹⁹ W.H. Press, S.A. Teukolsky, W.T. Vetterling and B.P. Flannery, *Numerical recipes in C: The art of scientific computing* (Cambridge University Press, 1992).
- ²⁰ J. Z. Sun, Phys. Rev. B **62**, 1 (2000).
- ²¹ I. N. Krivorotov, N. C. Emley, A. G. F. Garcia, J. C. Sankey, S. I. Kiselev, D. C. Ralph and R. A. Buhrman, Phys. Rev. Lett. **93**, 166603 (2004).
- ²² M. I. Freidlin and A. D. Wentzell *Random Perturbations of Dynamical Systems* (Springer, New York, 1991).
- ²³ E. T. Whittaker, G. N. Watson, *A Course in Modern Analysis* 4th Ed. (Cambridge University Press, Cambridge, UK 1927).

²⁴ E. Wong and M. Zakai, Ann. Math. Statist. **36** (1965), p. 1560.

²⁵ In modeling thermal effects through stochastic contributions in a system like ours, we are interested in considering the white noise limit of a potentially colored noise process²⁴. Stratonovich calculus is then to be preferred over $\hat{\text{Ito}}$ calculus as ascertained by the Wong-Zakai theorem.

²⁶ We can allow ourselves the freedom to switch between expressions involving γ and ϵ . $\gamma^2 = \frac{|\epsilon|(D+1)}{D+|\epsilon|}$ is a monotonically increasing function of $|\epsilon|$ with the convenient property that $|\epsilon| = 1 \rightarrow \gamma = 1$ and $|\epsilon| = 1 \rightarrow \gamma = 1$. As such limits written in terms of γ and ϵ are equivalent.

Appendix A: Elliptic Integral Identities

The identities

$$e(x) \equiv xE\left(1 - \frac{1}{x^2}\right) = E(x) \tag{A1}$$

$$k(x) \equiv \frac{1}{x}K\left(1 - \frac{1}{x^2}\right) = K(x) \tag{A2}$$

can be immediately proven by considering the defining differential equation satisfied by $K(x)$, namely²³:

$$\partial_x K(x) = \frac{E(x) - (1-x)K(x)}{2x(1-x)}. \tag{A3}$$

Computing then explicitly the derivative of $k(x)$ using definition (A1) and rearranging, one finds that:

$$\partial_x k(x) = \frac{e(x) - (1-x)k(x)}{2x(1-x)}, \tag{A4}$$

in other words they satisfy the same differential relation.